Surface interaction calculations over the Gulf of Tonkin

By HERBERT RIEHL,[1] *Colorado State University, Fort Collins, Colorado, USA, and* ERNST AUGSTEIN, *University of Hamburg, Hamburg, Germany*

(Manuscript received August 1, 1972; revised version March 12, 1973)

ABSTRACT

Two steady-state situations over the Gulf of Tonkin during winter were selected for a detailed study of air–sea interaction in relation to observed cloudiness. In one case southeasterly winds prevailed, and skies were nearly clear. The cloudy situation was marked by strong outflow from the continent with very low cloud bases over the whole Gulf of Tonkin. The exchange of sensible and latent heat at the air–sea interface is calculated for these two cases, and deductions are drawn concerning the difference between the states of sky utilizing these calculations in conjunction with synoptic-scale convergence and divergence patterns.

Introduction

It has long been known that weather patterns in the Tonkin Gulf–southern China area provide a marked exception to those found in the winter trade and monsoon regions in every other part of the globe. There are eight comparable regions: the North and South Atlantic trade; the North and South Pacific trade; the northeast and southeast low-latitude winter regimes over Africa; the India–Arabia northeast monsoon; and the Australia–South Indian Ocean southeast monsoon. In all of these regions air moves equatorward, under conservation of potential vorticity, from latitudes of about 30° to latitudes 10° or less. With decreasing latitude the absolute vorticity of the low-level currents decreases. This is associated with horizontal divergence of mass and sinking motion, hence little convective cloudiness.

In contrast, as shown by ship observations for many years and by satellite photos recently, the Gulf of Tonkin–southern China area experiences very extensive cloudiness and frequent light rain or drizzle when winds blow southward from the Asiatic continent during the winter monsoon season. The cloudiness is so prevalent that this area has by far the worst weather conditions for its latitude in the cold season around the globe. Partial or complete clearing, however, tends to occur during intermittent periods of southeast to south winds. This is a curious reversal from what one might anticipate. Northerly winds cross toward warmer and southeast winds toward lower ocean temperatures. We would expect fog and low stratus with the latter, intermittent cumuli with the former. Yet the opposite is observed.

Factors on various scales of motion may be probed to interpret this anomalous situation. Among the controls, the exchange of heat and moisture at the air–sea interface is a parameter of interest. In the following we shall examine situations with protracted southeasterly and northeasterly flow in order to learn, as far as possible with the available observational material, what transactions took place at the interface and in what way they aid toward an understanding of the observed states of sky.

Examination of the winters of 1965–68 on synoptic charts showed three types of dominant flow patterns over the Gulf of Tonkin. Of these, monsoon outflow from China occupied 31 per cent of the time, rather less than anticipated and quite variable in occurrence. Reverse flow toward the continent occurred during 23 per cent of the time, most frequently in the late part of the season but on occasion also in December and January. The balance of the time was taken up with light and eddying motions in the Gulf.

[1] Present address: Institut für Meteorologie, Freie Universität, Berlin.

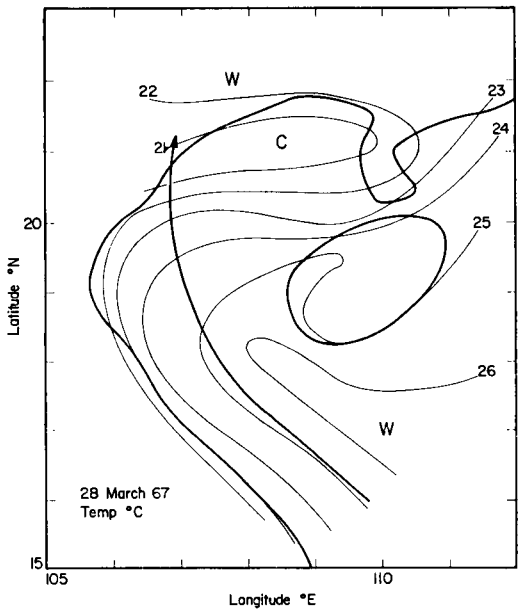

Fig. 1. Isolines of air temperature (°C) in the surface layer, 28 March 1967.

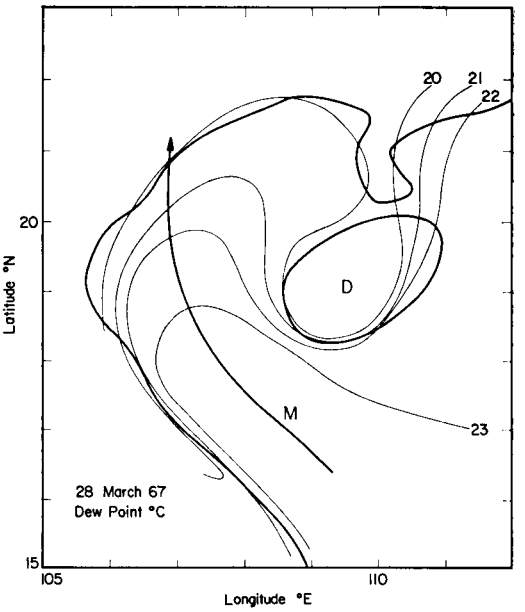

Fig. 2. Isolines of dewpoint (°C) in the surface layer, 28 March 1967.

The latter situations are not suitable for computations as here intended. However, the monsoon and reverse flow types, once established, tend to last at least 3–5 days and sometimes several weeks. A true steady state over long periods is then established, very suitable for many forms of research, including our own. Surface wind velocities are on the order of 15–20 knots or more; there is little eddying, and successive streamline charts parallel one another almost completely. Thus it is possible to "composite" episodes of several days' duration during monsoon or reverse flow and thereby stabilize and augment the observational material for computation. Surface and upper air charts, distributions of temperature in air and sea, and cloudiness and humidity are similar for comparable episodes. It is considered representative therefore, to select one episode for each flow pattern and to present the interface calculations as typical. In view of the very large differences between the two basic flow types any inhomogeneity within each of the two groups is considered relatively minor.

Data for surface maps were furnished by three-hourly reports from numerous ships over the Gulf of Tonkin plus Chinese coastal reports on the mainland and Hainan Island. Over the sea, where diurnal variations are slight, observations from 00-09Z and from 12–21Z were plotted together to give as much stability as possible to successive analyses. Upper air data were transmitted by various stations around the Gulf of Tonkin. Principal use will be made of rawinsonde observations taken at two quasi-stationary positions over water: at 20° N 107° E, labelled "NS"; and at 18° N 107.5° E, labelled "Y".

Southeast flow 26–30 March 1967

Situations with surface winds between southeast and south, usually curving slowly clockwise toward the Chinese coast, may persist for several days, and even a week or more, over the Gulf of Tonkin in the middle of winter, although their frequency is highest in late winter and spring. The example chosen is typical for wind and weather as observed in this group of cases.

Description. Figs. 1 and 2 are examples of temperature and dew-point analyses for a particular 12-hour period. Marked gradients along the streamline are evident, as well as the influence on the whole pattern exercised by Hainan Island. In Fig. 3 a selection of ship and Chinese

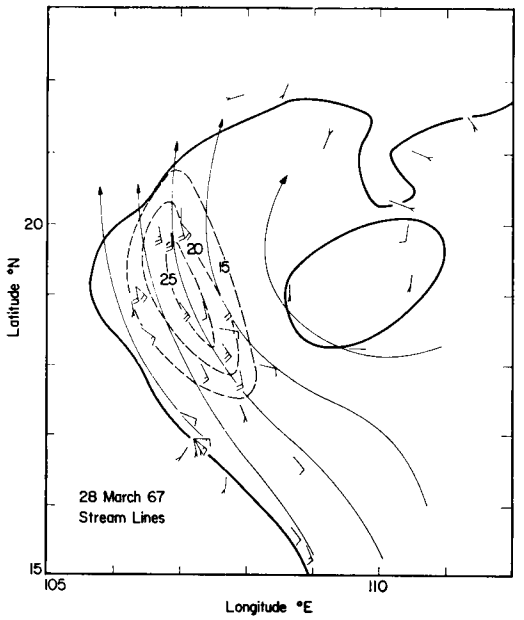

Fig. 3. Streamlines and isotachs (kts) in the surface layer, 28 March 1967.

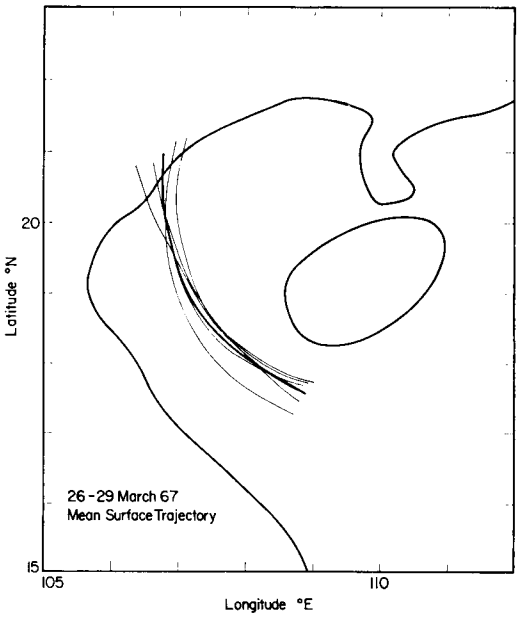

Fig. 4. Plots of central streamline and resulting mean surface trajectory, 26–29 March 1967.

winds is shown, together with streamlines and isotachs. The decrease of wind speed toward the Chinese coast is hypothetical: it has been drawn to conform to the low Chinese wind speeds farther east.

Variations in the orientation of the central streamline were slight during the period so that an average streamline (the heavy streamline in Fig. 4), may be regarded as a steady-state trajectory. Profiles of air-mass property can be drawn from the analyses along this trajectory, illustrated in Fig. 5 for dewpoint temperature. Again, variations between individual maps are slight and well within the range of error in drawing isotherms; hence, an average dewpoint gradient along the trajectory can be established. Fig. 6 shows profiles of air temperature (T_a), dewpoint (T_d), wind speed (V_0), and ocean-surface temperature (T_0) following the trajectory. The latter was taken from a single chart

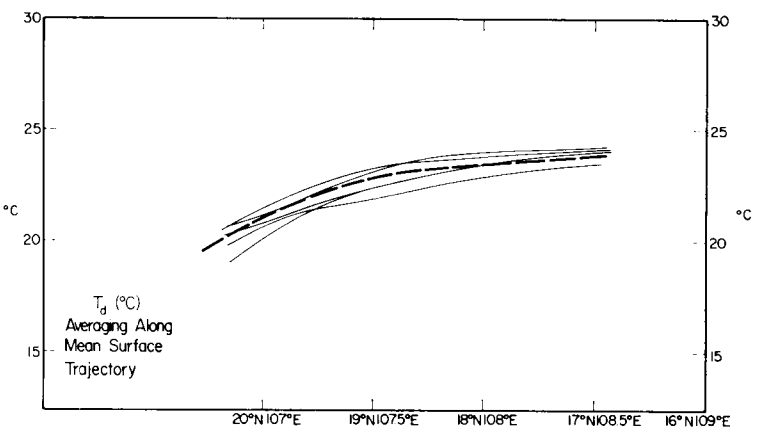

Fig. 5. Profiles of dewpoint temperature (°C) in the surface layer along the mean trajectory of Fig. 4 and averaged profile (dashed).

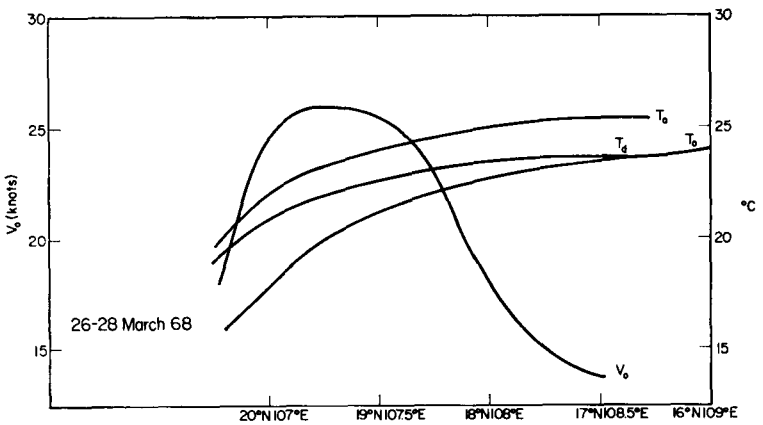

Fig. 6. Average profiles of air temperature, dewpoint, wind speed, and ocean temperature along the mean trajectory of Fig. 4, 26–29 March 1967.

of T_0 which was composited for the whole period of analysis. It is of interest that $T_0 - T_a$ and, especially, $T_0 - T_d$ increase downstream, whereas $T_a - T_d$ decreases only very slowly without coming close to zero.

Exchange of heat and moisture at the interface. In normal tradewind situations exchanges of heat, moisture, and momentum between sea and air usually can be made with some success using the turbulence method with equal exchange coefficients at nearly neutral stability. For the present case, with strong stability near the interface as indicated from $T_0 - T_a$ in Fig. 6, such a procedure does not appear appropriate. An alternative is furnished by a budget calculation. Fortunately, the trajectory passed close to both quasi-stationary ship positions. At these locations, wind direction and speed remained constant with height for about 400 m, followed by slow clockwise turning (Fig. 7). The assumption of two-dimensional flow appears valid to 960 mb and marginal to 950 mb, or to a height of 600 m above the sea. Near 950 mb the top of a dry inversion is found at both stations after averaging the soundings at 00 GMT for four days.

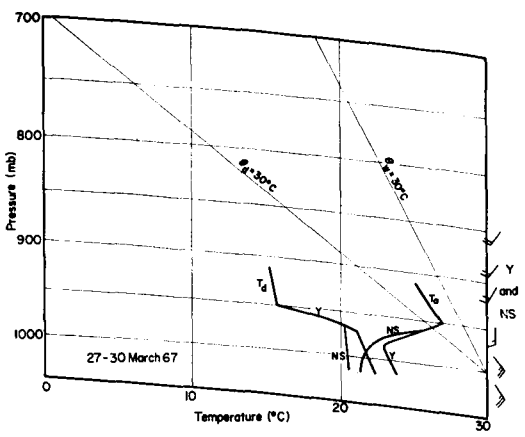

Fig. 7. Tephigram of temperature and dewpoint at stations Y and NS; averages for 26–30 March 1967, 00 GMT. Dry and moist adiabats of 30 C are indicated by θ_d and θ_w.

From mass continuity a sinking of 20 mb must have occurred, following the top of a column over the distance of 230 km from Y to NS, in view of the increase in wind speed from 17 to 25 kts, assuming constant streamline spacing as suggested by Fig. 3. This would lower the top to 970 mb, at which pressure the averaged profiles at NS being to depart downward from those at Y. We shall at first perform computations assuming that such sinking took place and, in a later section, consider how the inversion top itself may remain constant in spite of the sinking motion. Skies were completely clear along the trajectory; this simplifies the calculations.

From continuity the mass flow (M) is given by

$$M = \frac{1}{g} V \, dp \, \delta n = \text{const} \ (s) \qquad (1)$$

where s and n are coordinates oriented parallel and perpendicular to V, the velocity; g is the

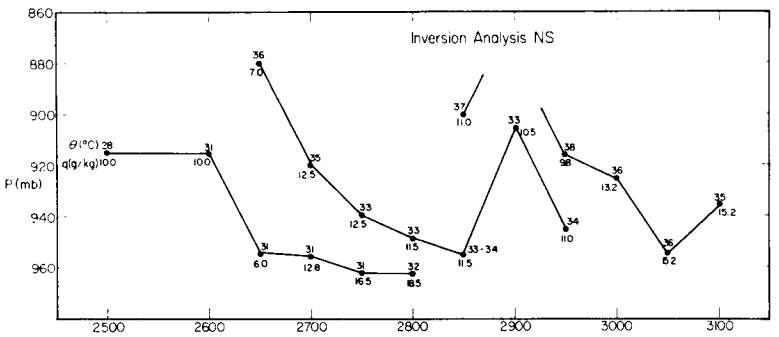

Fig. 8. Inversion-top analysis at NS 25–31 March 1967. Potential temperature (°C) and mixing ratio (g/kg) are plotted above and below each point, respectively. Three separate inversions are in evidence, gradually lowering and eventually disappearing below 950 mb. Date and time (GMT) at bottom.

acceleration of gravity; and dp is the variable pressure thickness of the layer considered. With the assumption of a material top, the divergence of sensible and latent heat transfer in the layer below the inversion is closely given by:

$$\int Q_s \, \delta s \, \delta n = c_p M(\hat{\theta}_2 - \hat{\theta}_1) \tag{2}$$

and

$$\int Q_e \, \delta s \, \delta n = L M(\hat{q}_2 - \hat{q}_1) \tag{3}$$

Here, Q_s and Q_e denote sensible and latent energy transfer per unit area of the interface (negative values indicate a heat flux to the ocean); c_p denotes specific heat at constant pressure; L the latent heat of evaporation; θ potential temperature; and q specific humidity. The "hats" indicate averaging over the pressure depth dp; the subscripts "2" and "1" refer to the end point and starting point of the trajectory, respectively.

We find that $M = 4.2 \times 10^4$ g/sec, $\hat{q}_2 - \hat{q}_1 = -2$ g/kg, $\hat{\theta}_2 - \hat{\theta}_1 = -2$ C, $Q_s = -72$ ly/day, and $Q_e = -180$ ly/day. The condensation on the ocean surface is 0.3 cm/day. The total energy flux $Q_a = Q_s + Q_e = -250$ ly/day, heat added to the ocean.

Inversion analysis. We shall now consider the question how the inversion base maintains its average altitude against the sinking motion and whether a transfer of air takes place through the mean inversion. Individual soundings show fluctuations in inversion structure illustrated in Figs. 8 and 9 for inversion tops.[1] In general, these tops could be identified readily by their potential temperatures at both stations. Potential temperatures are nearly identical; they increase to remarkably high values over the five-day period, shown in a succession of three inversions, all of which undergo net sinking motion

[1] Variations over periods shorter than twelve hours cannot, of course, be detected.

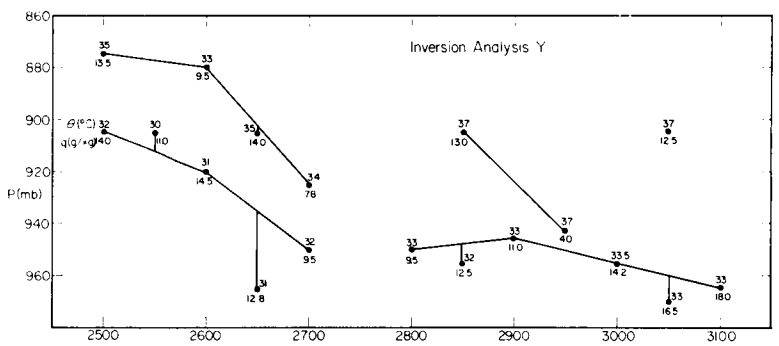

Fig. 9. Inversion analysis at Y, 25–31 March 1967. Notation as in Fig. 8. Soundings at 12 GMT (20 local) connected by vertical lines.

and eventual loss of identity when they drop to 950–960 mb.

The changes of specific humidity following a particular inversion are more difficult to interpret. Whereas potential temperature remains nearly constant and serves as an excellent identifier of an inversion, specific humidity changes erratically—though, on the average, it increases with lowering inversion height. Thus, total energy is not conserved following an inversion before it begins to make contact with the surface southeasterly flow upon dropping to 950 mb. We must conclude that the moisture variations are in no way related to exchanges with the air near the ocean surface, but that they must reflect processes that had taken place when the air crossed the Annam Mountains to the west or the country beyond those mountains.

For our purposes it appears relevant, solely, that all inversions vanish when reaching 950–960 mb, or 600 m height. It is plausible to suggest that turbulent motions in the lower layer extend upward to this altitude and there begin to incorporate the air from the inversion into the lower layer—subtracting sensible heat and adding moisture, as in the case of trade-wind inversions (Riehl et al., 1951; Augstein, 1971) but as a dry process. With this postulate, the maintenance of the average inversion height at 950 mb can be understood. It is remarkable that turbulence in the surface layer should reach to 600 m which is almost exactly the top of the trade-wind subcloud layer with nearly adiabatic lapse rate. Presumably, this turbulence is maintained from the energy of the mean motion; such a conversion must take the place of buoyancy in the trades. Production of horizontal kinetic energy is 1×10^6 ergs/g from the pressure drop following the air moving from Y to NS. The actual increase of kinetic energy amounts to half of the generation. Thus, the other half is used to do work against friction at the ground and, presumably, within the layer below the inversion. A similar partition was computed by Riehl (1963) for hurricanes.

Conclusion. The dual effect of latent plus sensible heat transfer to the sea, coupled with slow intrusion of warm air from above, appears to be responsible for holding $T_a - T_d$ virtually constant and for preventing fog formation. Synoptic-scale mass divergence and sinking is related to the gradual lowering of successive dry inversions until they come in contact with the surface turbulence, incorporating the inversion air into the surface layer.

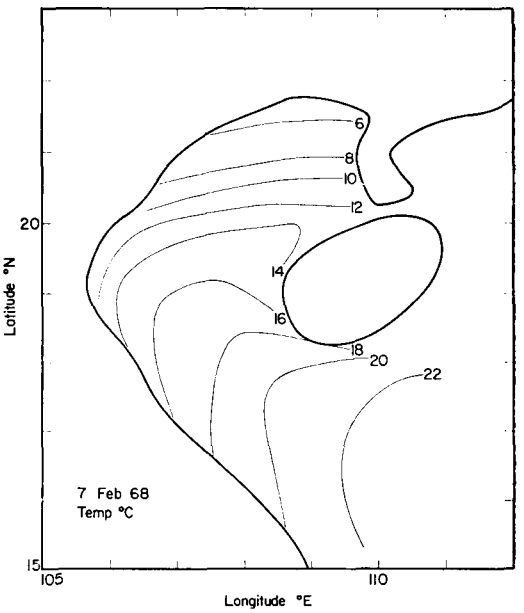

Fig. 10. Isolines of air temperature (°C) in the surface layer, 7 February 1968.

It may be added that satellite pictures, taken around noon local time, showed a small cloud area, presumed to be mostly fog, close to the North Vietnam coast on each day. Ships situated about 19–20° N 106° E recorded fog each morning, clearing in the afternoon. The strong winds noted at NS were not found at the western edge of the Gulf (Fig. 3). There, winds were frequently quite light and variable during the morning, while the southeasterly flow appeared to reach the shore in the afternoon—no doubt as part of the sea-breeze circulation. Fig. 3 suggests that a stationary area of convergence (on and just off the shore, and produced by the slowing down of the wind approaching the land) stopped the sinking of the dry and potentially very warm air at the inversion top. With slow wind speeds, an adjustment of T_a and T_d to T_0 can occur. Moreover, a stratus deck may form and build down to the sea through evaporation of falling drops and recondensation.

Northeast monsoon 6–8 February 1968

We shall now examine the "normal" situation—equatorward outflow from the continent.

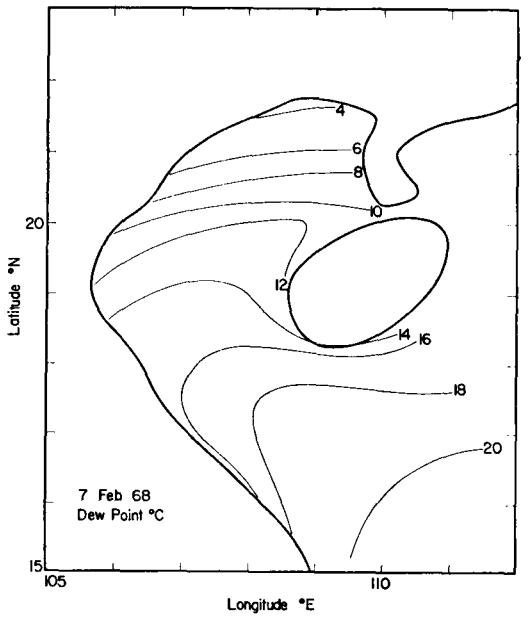

Fig. 11. Isolines of dewpoint (°C) in the surface layer, 7 February 1968.

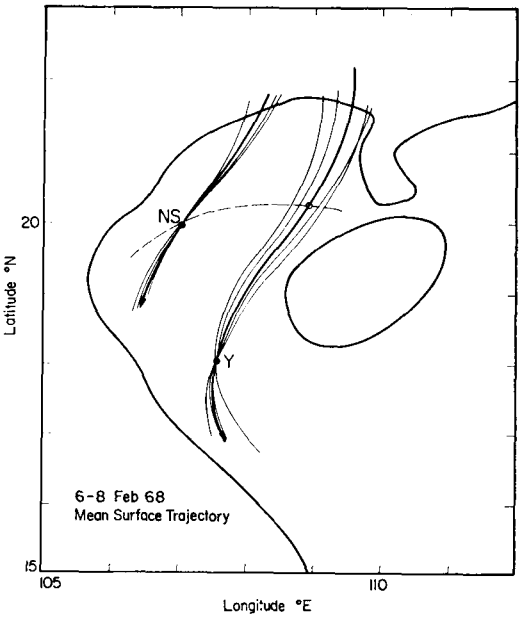

Fig. 13. Surface trajectories ending at NS and Y, 6–8 February 1968, and displacement of NS station to averaged trajectory ending at Y. The dashed line is parallel to the sea-surface isotherms of Fig. 14.

Almost the whole of February 1968 was characterized by persistent strong monsoon; the days analyzed here are a representative sample.

Description. Figs. 10–12 show typical maps of air temperature, dew point, and wind, just as for the previous series. The counterclockwise turning of the monsoon over the Gulf of Tonkin toward the south, no doubt enforced by the Annam Mountains and the island of Hainan, is regularly observed. In this type of situation, as in the previous one, successive streamline charts show a very steady picture that can be approximated by a mean trajectory (Fig. 13); however, the trajectories do not pass through both Y and NS. In order to be able to make calculations, the NS soundings must be shifted to a representative position along the trajectory leading through Y. Fig. 13 shows how this shift was made along constant ocean temperature (Fig. 14). It is seen that the distances from land to the actual and shifted NS positions are about equal, and that the same amount of oceanic temperature gradient is traversed. Probability is, therefore, high that the NS soundings are representative of what a ship station would have observed at the shifted position. Nevertheless, the shift clearly introduces an assumption, and much of the following analysis is subject to its validity.

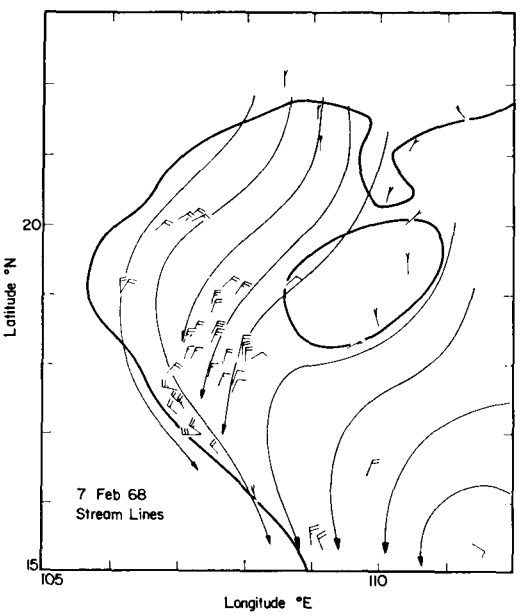

Fig. 12. Streamlines in the surface layer, 7 February 1968.

Independent of this assumption are the profiles of Fig. 15, constructed as for Fig. 6.

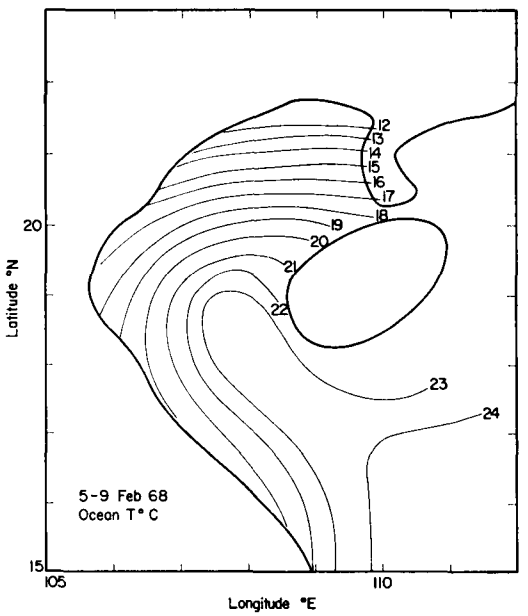

Fig. 14. Sea-surface isotherms (°C), 5–9 February 1968.

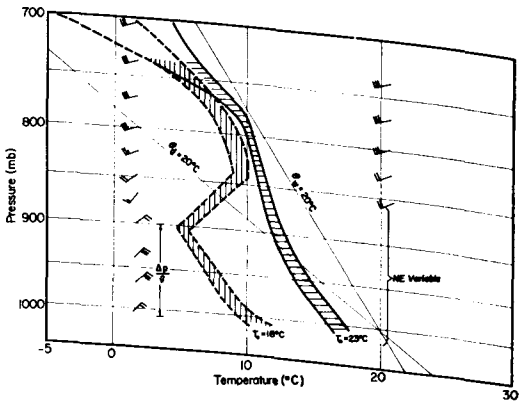

Fig. 16. Tephigram of temperature and dewpoint at NS and Y stations, averaged for 6–8 February 1968. Shaded areas denote observed cloud thickness. Column marked $\Delta p/g$ denotes thickness of inflow layer at NS.

Fortunately, the NS surface data fit on these profiles exactly. We observed that $T_0 - T_a$ is constant and very large at 6C; also, that $T_a - T_d$ is very small and roughly constant at 1 C. It follows that a very low cloud base overlies the whole Gulf. Often this cloud base becomes so low that widespread intermittent reports of fog over the Gulf are common, especially along its western side.

Fig. 16 shows mean soundings for the two stations averaged over three days. The layer filled by cloud is indicated by shading. It extends from near the surface to above 750 mb at both locations; $T_a - T_d$ as indicated by the soundings, corresponding to relative humidity of 95 percent, would become zero if saturation with respect to salt solution were considered.

At NS we find a strong inversion completely filled with cloud. Below the base the lapse rate is moist adiabatic in the northeast winds. Wind direction changes sharply to southwest in the inversion layer. With increased altitude clockwise turning becomes small, while wind speed increases slowly upward. Where the clouds end there is, as a rule, no wind shift and no secondary stable layer on individual soundings, as well as on the mean sounding of Fig. 16.

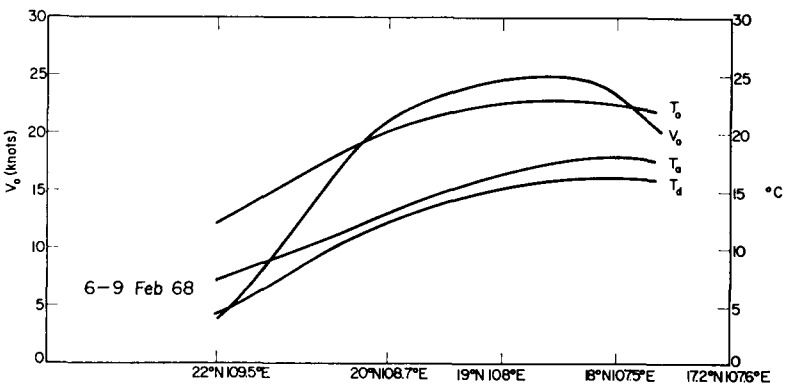

Fig. 15. Average profiles of air temperature, dewpoint, wind speed, and ocean temperature along the assumed mean trajectory of Fig. 13, 6–8 February 1968.

Table 1. *Comparison of interface fluxes determined by several methods, 6–8 February 1968 (units: ly/day)*

	Q_s	Q_e	Q_a	E	Q_s/Q_e
Divergence of transport			1 930		
Trubulence formulae (adiabatic)	240	590	830	1.0	0.41
Turbulence formulae (adjusted for instability)	540	1 250	1 790	2.1	$R =$ 0.43
Divergence of transport (Q_a adjusted to column above. The values of Q_s and Q_e in parentheses are calculated values based on the assumption of no phase changes)	(730)	(1 060)	1 790	(1.75)	$R' =$ (0.69)

At Y station, the inversion is replaced by a stable layer, also completely cloudy, mainly through heating of the layer below 850 mb on the way from the (shifted) NS position. The northeasterly winds are somewhat deeper, and with a variable top. A definite shift to the southwest occurs at 850 mb, which, together with the marked stability above this level, indicates the height to which turbulent transport in the monsoon layer may be expected to extend. This height also corresponds closely to the top of the monsoon layer computed from conservation of potential vorticity along the trajectory. From Figs. 12 and 13 relative vorticity changes from clockwise to counterclockwise, overbalancing the small decrease in latitude.

Exchange of heat and moisture at the interface. Assuming parallel streamlines, calculations of the interface transfer of heat and moisture can again be accomplished using equations 1–3. We have $\hat{V} \leq 12.5$ m/sec at NS and 8.6 m/sec at Y; $dp/g = 110$ and 160 g/cm², respectively; therefore, $M = 1.37 \times 10^5$ g/sec. Further, $\hat{q}_2 - \hat{q}_1 = 11.0 - 6.5 = 4.5$ g/kg and $\hat{\theta}_2 - \hat{\theta}_1 = 20 - 12 = 8$ C. Then, divergence of latent heat is 3.7×10^5 cal/sec, that of water vapor is 6.2×10^2 g/sec, and that of sensible heat is 2.57×15^5 cal/sec. Using equations 2 and 3 combined, with a distance s of 280 km between stations in this case, and $n = 1$ cm as before, $Q_a = 1\,930$ ly/day for conservation of energy neglecting radiation. This is a rather high value, but not unusual under similar circumstances.

In the previous case we omitted direct calculations of energy flux using turbulence formulae at the ocean surface because of the great stability. In the present instance poor results should again be expected; this time because of thermal instability. Nevertheless, the calculations were made, mainly as a guide for subsequent modifications. For the adiabatic case:

$$Q_s = \varrho c_p c_D (T_0 - T_a)\, V_0 \tag{4}$$

and

$$Q_e = \varrho L c_D (q_0 - q_a)\, V_0 \tag{5}$$

Here ϱ, the density of air, is 1.15×10^{-3} g/cm³; the drag coefficient c_D was taken as 1.15×10^{-3}. The other quantities are given by Fig. 15. We obtain $Q_s = 240$ ly/day, $Q_e = 590$ ly/day, $Qa = 830$ ly/day, and $E = 1$ cm/day. The total energy flux falls short by a factor greater than two of that needed for energy balance; and, in this case, the difficulty must be ascribed to the assumptions inherent in equations 4 and 5 rather than to the margin of error in computing the flux divergences.

In a second estimate the large instability was considered by utilizing the method of Dyer (1967) and the approximation of Hoeber (1969) for the formulae of Monin & Obukhov (1954). Results are: $Q_s = 540$ ly/day, $Q_e = 1\,250$ ly/day, $Q_a = 1\,790$ ly/day, $E = 2$ cm/day and $Q_s/Q_e = 0.43$. This calculation is clearly compatible with the flux divergence. Adjusting the latter to 1 790 ly/day for energy balance, the export from the volume would require an equivalent $Q_s = 730$ and a $Q_e = 1\,060$ ly/day, assuming no changes of phase. For comparison, all computational results are given in Table 1.

Models of the monsoon stratus. If it is granted that the lowest two lines of Table 1 are correct, the maintenance of the overcast and of the very low ceilings over the Gulf of Tonkin may be examined further, mainly by comparing Q_s/Q_e from the interface calculation and from the

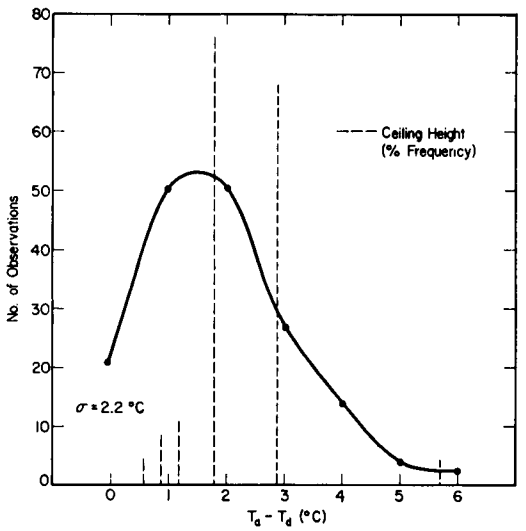

Fig. 17. Frequency distribution of ceiling height computed from $T_a - T_d$, 6–8 February 1968, assuming mixed subcloud layer; and percent frequency distribution (inner scale on ordinate) of estimated or measured ceiling heights (dashed) plotted at $T_a - T_d$ corresponding to the same heights for the mixed layer.

budgets of heat and moisture under the assumption of no change in phase. The former quantity will be designated R and the latter R'. The first hypothesis was that water falling out from the return current above 850 mb evaporated partly or wholly before reaching the sea, in this way building down the cloud constantly and abstracting sensible heat from the air, maintaining the large $T_0 - T_a$. If this took place we should find that $R > R'$; i.e. more water vapor and less sensible heat would flow out than supplied by the ocean surface, pointing to the requirement for a secondary moisture source. Clearly, this attractive hypothesis fails.

The alternate hypothesis, which must be true, is that a fraction of the evaporated ocean water recondenses; namely, 190 ly/day from Table 1. Since divergence of water transport may be neglected as a small quantity, precipitation of approximately 3 mm/day must occur for $R' > R$ as computed. A survey of all hourly and three-hourly ship observations showed that light rain or drizzle was reported in 40 per cent of the reports. Hence, an area average of 3 mm/day is very likely to be an accurate estimate. Lacking a network of rain gauges over sea, comparison with direct measurements cannot, of course, be made.

In spite of the general overcast and low ceiling, there are nevertheless mesoscale variations. An attempt was made to obtain some data on this mesostructure, at least statistically, by examining ceiling height and $T_a - T_d$ for 170 observations which were available in the area during the period of study. In the case of a completely mixed subcloud layer there should be an equivalence between ceiling height as computed from $T_a - T_d$ and as taken from direct observations. Fig. 17 shows the frequency distribution of ceiling height from $T_a - T_d$, and the percent frequency distribution of observed heights plotted at the values of $T_a - T_d$ which correspond to these heights. Correspondence between the two sets of data is not outstanding; but it is nevertheless fair when one considers that the subcloud layer is not always completely mixed, that most ceiling heights are estimated and they must be reported according to a fixed code.

For our purposes the main result is that a sizeable standard deviation does occur (2.2 C for $T_a - T_d$), so that one can think of a mesoscale eddy model with ceilings alternately higher and lower than the mean. In part of an eddy air is heated from below, with an increase in temperature lapse rate. Ascending motion with condensation would be concentrated there. In other parts of the eddy some of the condensed water may slowly settle out. Where this water comes down, possibly connected with downdrafts, the cloud base is built down toward the ocean. The heat of condensation will, thus, remain in the upper part of the cloud while the lower evaporation subtracts heat, thereby leading to the absolutely stable lapse rate conducive to perpetuation of the stratus-type overcast.

Southern limit of stratus. Both at NS and Y the equivalent potential temperature (θ_e) at the top of the inversion is 330–332 K, and this essentially represents the heat content of the monsoon return flow as given by the winds in and above the inversion. At the surface $\theta_e = 308$ K at NS and 326 K at Y. There the absolute stability is much weaker than at NS. Values closely approach 330–332 K attained by the monsoon before returning, at least in part, over its own southward trajectory at a higher altitude.

The absolute stability vanishes to great

heights when T_a reaches 19–20 C at $T_a - T_d = 1$ C. Freer vertical motions, both up and down, can then develop because of buoyancy forces. The downdrafts will bring slightly warmer and drier air toward the surface. As a result, $T_a - T_d$ can begin to increase; the cloud base can rise, and the stratus will give way to cumulus clouds.

Actually, the solid stratus, as observed by satellite, does not extend southward of 17–16° N; rather, it terminates at this latitude along a well defined edge with ENE–WSW orientation with trade-wind cumuli farther south. This edge coincides with surface temperatures of 20–22°C in mid-winter, hence, with some vertical instability with regard to saturated adiabatic processes as described above.

Conclusion. The foregoing description for maintenance of the low stratus overcast suggests that the mass convergence in the southward-moving current is the major factor in protecting individual air columns on their path. Thus, the interface and mesoscale physical processes here deduced can occur without hindrance and lead to the observed steady state on the synoptic scale. Even though rain falling from the return flow in and above the main stable layer or inversion does not appear to be essential for maintaining the very low cloud base, the lower layer is, nevertheless, shielded from the effects of such subsidence and admixture of dry air as occurred in the March 1967 case. It is concluded that synoptic-scale flow and divergence patterns appear to play a key role in determining low cloud formation over the sea, overriding in importance even the interface processes.

Acknowledgements

This paper is based on work carried out in conjunction with the former Weather Research Facility of the United States Navy. Special acknowledgement is due to the commanding officer of the Facility at that time, W. L. Somervell, Jr.

REFERENCES

Augstein, E. 1972. Mass and heat budget estimations of the Atlantic SE trade wind flow at the Equator. *Met. Forsch. Ergebn. B 8*, 31–41.

Dyer, A. J. 1967. The turbulent transport of heat and water vapour in an unstable atmosphere. *Quart. J. Royal Met. Soc. 93*, 501–508.

Hoeber, H. 1969. Wind, Temperatur und Feuchteprofile in der wassernahen Luftschicht über dem äquatorialen Atlantik. *Met. Forsch. Ergebn. B 3*, 1–26.

Monin, A. S. & Obukhov, A. M. 1954. Fundamental laws of turbulent mixing in the atmospheric layer near the ground. *Trudi Geofis. Inst. Acad. Nauk USSR 24*, 163–187.

Riehl, H., Yeh, T. C., Malkus, J. S. & La Seur, N. E. 1951. The northeast trades in the Pacific Ocean. *Quart. J. Royal Met. Soc. 77*, 598–626.

Riehl, H. 1963. Some relations between wind and thermal structure in steady state hurricanes. *J. Atm. Sci. 20*, 276–287.

ВЫЧИСЛЕНИЯ ВЗАИМОДЕЙСТВИЯ АТМОСФЕРЫ И ОКЕАНА ДЛЯ ТОНКИНСКОГО ЗАЛИВА

Для детального изучения взаимодействия атмосферы и океана в связи с наблюдаемой облачностью были выбраны две зимних квазистационарных ситуации над Тонкинским заливом. В одном случае господствовали юго-восточные ветры и небо было почти чистым. Облачная ситуация была отмечена сильным оттоком масс с континента с очень низким уровнем основания облачности над всем Тонкинским заливом. Для этих двух случаев рассчитан обмен теплом и скрытой теплотой на поверхности раздела океана и атмосферы. С помощью этих вычислений вместе с анализом конвергенции и дивергенции воздушных масс синоптического масштаба сделаны заключения о роли состояния неба для исследуемого обмена.